REQUIREMENTS FOR EFFECTIVE HIGH LIFT CFD

F.T. Lynch*, R.C. Potter* and F.W. Spaid†
McDonnell Douglas Corporation

ABSTRACT

Development of effective CFD capabilities for analyzing complex 3-D high-lift systems for subsonic transports is presently a high industry priority because of the potential benefits in reduced design cycle time and ability to define more cost- and performance-effective concepts. One of the key enabling technologies required to achieve this capability is the development of turbulence models, etc., which more appropriately represent the very complex flow physics involved. To assess the current status of state-of-the-art CFD methods regarding the ability to adequately represent some of these complex flow situations, results from a comprehensive 2-D experimental program investigating multielement high-lift airfoil characteristics, as well as results from a corresponding CFD calibration study, are reviewed. Specific issues addressed include the influence of spreading and merging shear layers and wakes, and flow separation on the flap at approach conditions. Current CFD capabilities to predict these effects are assessed, which then leads to a recommendation for further near-term 2-D development of these aspects concurrent with other 3-D specific tasks.

INTRODUCTION

Remarkable progress has been made in the development and successful application of modern high-fidelity CFD methods for the aerodynamic design and optimization of subsonic transport cruise configurations[1,2]. Currently available methods provide quite accurate predictions for moderately complex geometries at attached-flow cruise conditions, and the use of constrained inverse CFD techniques permits the rapid and early definition of cost-effective and high-performance aerodynamic designs that are certain to achieve target cruise drag characteristics in flight. Significant progress is also being made in the development and application of advanced CFD methods addressing cruise-configuration design conditions involving 3-D separated flows, i.e., at buffet onset, etc. Consequently, the aerodynamic design cycle time required for the definition and documentation of effective, low-risk cruise configurations has been shortened significantly. In this modern process, wind-tunnel testing complements the CFD role by more efficiently securing the very large quantity of data required in the detailed production development process once the aerodynamic configuration has been established[1]. And, advanced testing techniques, such as the use of pressure sensitive paint, are also being used to shorten this experimental portion of the process.

Unfortunately, a similar effective role for CFD does not exist in the current aerodynamic design and development process for low-speed, multielement-high-lift systems on subsonic transports. In this case, the much more complex geometries and flow physics issues involved present sizable obstacles to aerodynamic analysis using existing computer and flow-modeling resources. As a result, the existing design process relies almost exclusively on costly and lengthy wind-tunnel development testing. Hence, the lack of effective high-lift CFD capabilities necessitates a significantly longer aerodynamic design cycle time than needed for the cruise configuration development, and most certainly does not permit definition of the most cost- and performance-effective high-lift system designs. Also, the lack of insight resulting from the absence of effective high-lift CFD capabilities does lead to a significantly higher risk of encountering "surprises" at full-scale flight conditions that require further costly development and aircraft rework. Consequently, in order to overcome the shortcomings of the current high-lift system design process, a major effort is now being focused on the development of effective CFD capabilities for analyzing 3-D high-lift systems.

To be effective, the resulting CFD methods must be capable of quickly modeling the very complex 3-D multielement geometries involving segmented

* Long Beach, CA
† St. Louis, MO

leading- and trailing-edge devices, large wing-mounted engine installations, and flow-control devices such as strakes and vortex generators. These methods must also be capable of accurately representing very complex flow physics situations which will be encountered involving merging shear layers with off-body flow reversals, vortex/viscous interactions, interactions between the engine exhaust jet and the flap, flows with strong 3-D viscous flow components, strong compressibility effects (on the slat), receptivity influences on boundary layer transition, relaminarization, etc. The product-design user community will demand that these CFD methods be robust and easy to use, be fast for quick turnaround, be able to provide meaningful predictions of lift, drag, control, and (eventually) aeroacoustic characteristics, be able to accurately predict component rigging effects and guide the tailoring of the high-lift devices around the engine installation, and be able to provide reliable guidance for effective application of various flow control concepts.

Some of the enabling technology advancements needed to achieve the required high-lift CFD capability include automated grid generation for these complex 3-D geometries, solution-adaptive grid capabilities for tracking vortex flows and wakes, CFD algorithm advancements to provide at least an order of magnitude reduction in solution times, and the development of turbulence models appropriate for merging shear layers, vortex flows, flows with strong 3-D viscous components, varying Reynolds number, etc. Although the largest part of the challenge to be addressed involves the complex 3-D geometries and the correspondingly complex 3-D flow physics, it is more tenable to initially examine some of the crucial CFD issues at 2-D conditions where the problems are clearly more tractable. The 2-D solutions will then form the basis for the development of their 3-D counterparts. Crucial issues which fall into this category are the modeling of the merging shear layers with eventual off-body flow reversal at maximum lift conditions in the approach and landing configuration, addressing possible flow separation on the flap at approach conditions, slat compressibility effects, Reynolds number effects, and receptivity effects on transition.

To facilitate the understanding of the complex flow physics issues dominating the aerodynamic performance of multielement high-lift airfoils, to provide a comprehensive set of data needed to properly assess current CFD capabilities, and to identify areas where advancements are necessary, a unique high Reynolds number test program is being conducted, utilizing a 2-D, transport-aircraft-type multielement, high-lift airfoil design[3-7]. Extensive diagnostic data are being obtained as part of this program, including effects of slat and flap rigging changes[8-12]. This paper begins with a review of the more important experimental results in order to identify the flow mechanisms currently limiting the performance of such multielement airfoil designs, and thereby identify critical features requiring accurate CFD predictions if the codes are to be useful in the design environment. Following this, predictions obtained using a current state-of-the-art CFD method are compared to the experimental database for the baseline geometry, and for two consequential geometry modifications, to qualitatively and quantitatively assess existing 2-D CFD capabilities, and to identify critical areas requiring additional development before all efforts are focused on the full 3-D problem.

2-D EXPERIMENTAL DATABASE

The three-element baseline geometry employed in this experimental study is illustrated in Figure 1. The cruise airfoil has a thickness ratio of 11.55%, and the slat and flap chords are 14.48% and 30% of the stowed chord, respectively. For the baseline geometry, both the slat and flap are deflected 30°, and the gap/overhang riggings are 2.95%c/-2.50%c and 1.27%c/0.25%c, respectively. The subject test program with this high-lift geometry is being conducted in the NASA Langley Low Turbulence Pressure Tunnel (LTPT)[13], which is a closed-throat, single-return wind tunnel which can be pressurized up to 10 atmospheres. The tunnel test section is 3.0 feet wide and 7.5 feet high, which, with the 22-inch (stowed) airfoil chord, results in a model aspect ratio of about 1.64. A sidewall boundary-layer control system utilizing the pressure difference between the tunnel and the atmosphere is employed to maintain 2-D flow. Details of this model installation have been published previously[14].

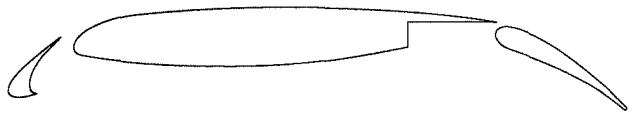

Figure 1: Typical Multielement High-Lift Airfoil

Instrumentation employed includes extensive chordwise static pressures, some spanwise static pressures to monitor maintenance of 2-D flow conditions, static pressures on the tunnel floor and ceiling to monitor wall effects, a wake-rake traverser system to measure drag, and a low-interference boundary-layer/wake traverser system with a flat-

tube pitot probe (for measuring near-surface boundary layer characteristics and determining skin friction levels). A (calibrated) hemispherical-shaped five-hole probe for assessing local total and static pressures (i.e., velocity) and flow angularity in the flowfield surrounding the multielement airfoil has also been employed. In addition to the foregoing pressure measurements, surface hot-film gages have been utilized to establish the boundary-layer state on each of the elements (i.e., laminar vs. transitional vs. turbulent), Preston-tube skin-friction measurements have been obtained[15], and hot wires have been employed for the measurement of unsteady velocity components (i.e., turbulence quantities). As with the model installation, details regarding the instrumentation and traverser system employed herein have also been previously published[8-12], and are therefore not repeated here.

Test conditions for this investigation have covered a relatively large range of Mach numbers and Reynolds numbers. Data have been obtained at freestream Mach numbers from 0.15 to over 0.3, and at (stowed) chord Reynolds numbers ranging from 5×10^6 to nearly 20×10^6. All of the results presented in this paper were obtained at a Mach number of 0.20, and for a chord Reynolds number of 9×10^6. The most complete data set has been obtained at these conditions, and the results obtained at these conditions are clearly representative. At this Mach number, local sonic velocities are reached at a pressure coefficient just beyond -16.

Chordwise static-pressure distributions on each of the elements of the baseline multielement airfoil geometry installed in the LTPT are displayed in Figure 2 for a range of angles of attack leading up to the maximum lift conditions (which occurs at 21°). For reference, 8° represents the corresponding approach condition, where lift generation and drag are both very important. Some features worthy of noting from these pressure distributions are as follows:

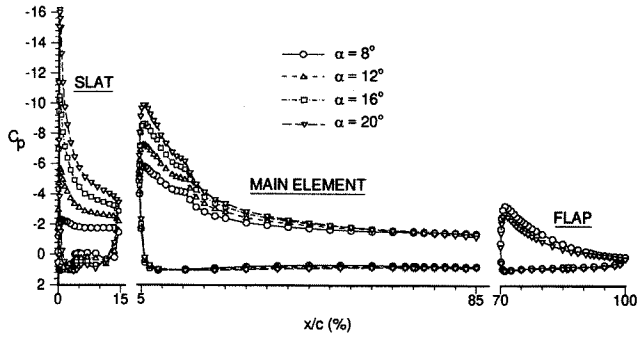

Figure 2: Element Static-Pressure Distributions

- The highest velocities occur on the slat, reaching sonic conditions just prior to reaching maximum lift.
- The most severe adverse pressure gradients also occur on the slat around maximum lift conditions.
- Pressure distributions on the slat upper surface are very flat at approach conditions, a condition conducive to maintaining laminar flow.
- The leading-edge loading on both the slat and the main element increases with increasing angle of attack, but not on the flap, where some reduction is noted.
- The upper-surface pressures on the slat and main element are not required to recompress as much as on the flap due to the presence of the following element.
- Extremely low velocities exist on the lower surface of each of the elements at all conditions.

The component and total lift values obtained by integrating these surface pressures are presented in Figure 3, with data shown for two separate test entries. Key lessons to be learned from these data include:

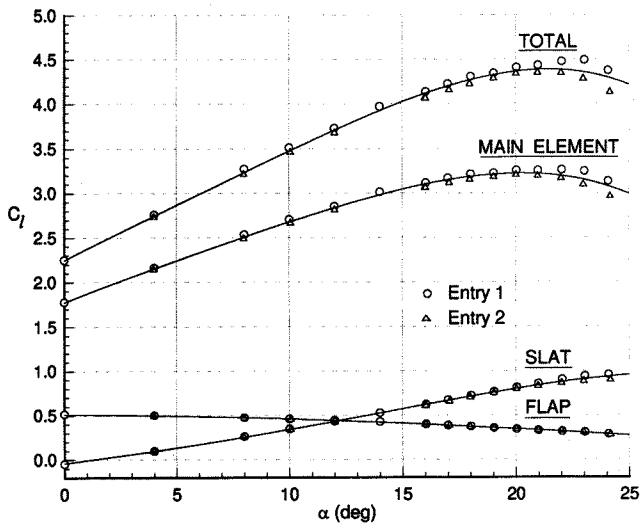

Figure 3: Baseline Component and Total Lift

- Maximum lift is established by an eventual reduction in the lift on the main element.
- The lift contribution from the flap itself decreases with increasing angle of attack, due primarily to a gradual unloading of the flap and to a very unfavorable normal force orientation.
- There is clearly some relatively small amount of scatter in the data from test to test, and the absolute magnitude of the pressure integrations has some as yet undefined potential integration error due to the relative coarseness of the spacing

between pressure orifices (compared to a normal computational grid).

Examination of the corresponding individual component normal-force distributions at approach conditions, maximum lift, and at an angle of attack just beyond maximum lift, presented in Figure 4, permits understanding of the phenomena limiting maximum lift with this baseline geometry. It can be seen that the lift reduction on the main element (beyond maximum lift) is caused by an unloading of the aft portion of the main element, which, in turn, appears to be caused by a rather dramatic unloading of the flap itself. This illustration clearly illustrates one of the primary functions of the flap in a multielement high lift system, namely to hold up the lift on the aft portion of the main element. In addition, it can be seen in Figure 4 that the slat normal force ceases to grow beyond maximum lift conditions, clearly implying a reduction in upwash due to the unloading of the aft portion of the multielement airfoil system.

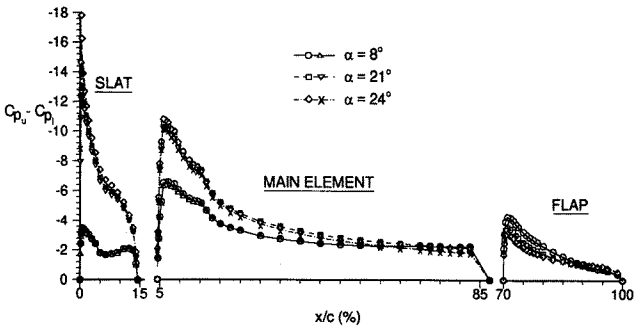

Figure 4: Element Normal-Force Distributions

Understanding of the flow physics controlling the aerodynamic performance of this high-lift geometry is enhanced considerably by examining results of additional diagnostic measurements. To start with, the boundary-layer state on each of the elements over the angle-of-attack range as derived from the surface hot-film gage measurements is summarized in Figure 5. Important points to be noted include the following:

- The boundary layer on the flap upper surface is turbulent right from the stagnation region at all angles of attack even though the local chord Reynolds number is quite low, likely as a result of unsteadiness in the wake of the main element.
- The boundary layer on the slat upper surface is predominately laminar at low angles of attack as expected, but the transition point moves to just aft of the suction peak as the angle of attack is increased.
- Boundary-layer transition on the main element upper surface also occurs just aft of the suction peak at angles of attack of interest.
- The boundary layer on the lower surface of each of the elements is mostly laminar at angles of attack of interest, with the exception of the flap at lower angles of attack, where the unsteadiness in the wake of the main element appears to somewhat limit the chordwise extent of laminar flow.

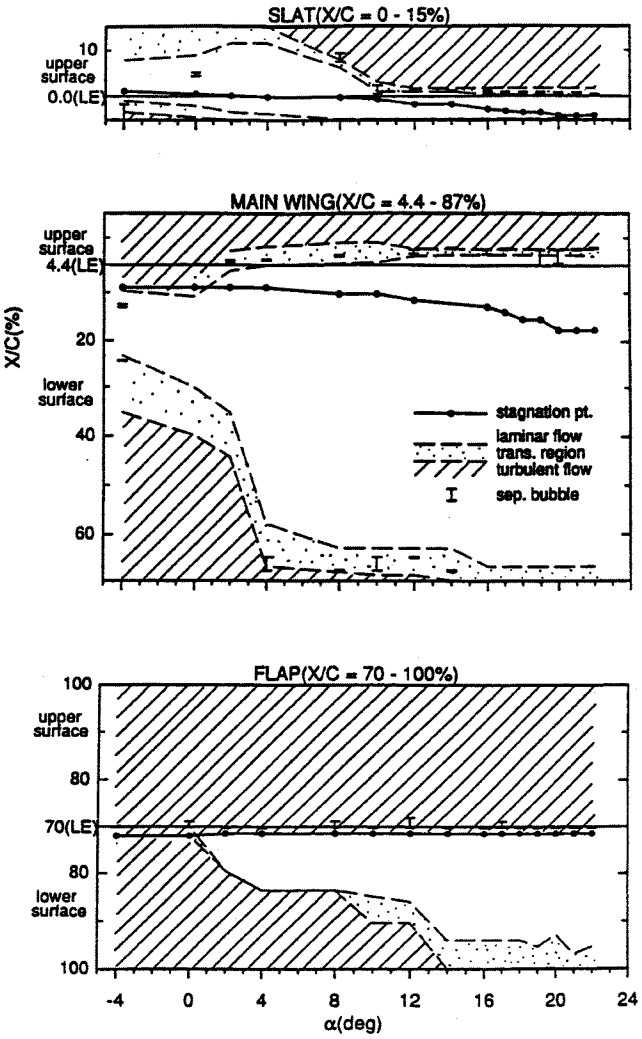

Figure 5: Hot-Film Transition Measurements

Local skin friction values estimated by using the Clauser technique[16] with the velocity profiles obtained from the flat-tube pitot probe over a range of angles of attack are shown in Figure 6 for three upper-surface locations, one near the trailing edge of the main element, and two on the flap. These results clearly show that the unloading of the flap and aft portion of the main element that is limiting maximum lift is not due to any on-surface flow separation, either on the main element or on the flap. The surface boundary layers are not even close to separation at maximum lift conditions. However, the boundary layer approaching the flap trailing edge is

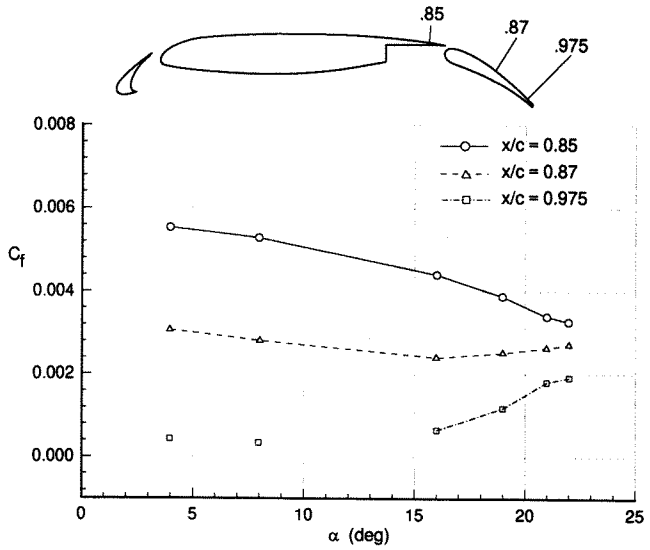

Figure 6: Main Element And Flap Skin Friction

very close to separation with this geometry at the lower (approach condition) angles of attack.

Since boundary-layer separation on the element surfaces is not an issue in controlling the maximum lift achievable with this three-element geometry, it becomes instructive to examine the off-body flowfield above the main element and flap, obtained with the five-hole probe, to help understand how the flowfield in this region can be causing the observed unloading of the flap and main element. Measured velocity profiles above the main element at two chordwise locations, and above the flap at two locations, are shown in Figure 7. Velocity profiles are presented for angles of attack of 8°, 16° and 21°, covering the range from approach conditions to maximum lift. The intermediate angle of attack is useful in permitting an assessment of the rate of growth of the momentum defect. Key observations which can be made from these data include the following:

- There is little evidence of a wake from the slat at 8°, even at the station just aft of the slat. This is not unexpected considering the relatively low velocities and extent of laminar flow on the slat at this condition.
- Even at the highest angle of attack, there is little evidence of merging between the slat wake and the main element boundary layer near the trailing edge of the main element.
- Spreading and merging of the slat and main-element wakes becomes very pronounced above the flap at maximum lift conditions.
- The velocity in the wake from the main element is approaching stagnation conditions at maximum lift near the flap trailing edge, and it is not difficult to imagine an extrapolation to reverse flow conditions at a slightly higher angle of attack.

Although not illustrated in Figure 7, another important characteristic to be noted is the existence of large and extensive normal static pressure gradients which exist in the region just aft of the main-element trailing edge.

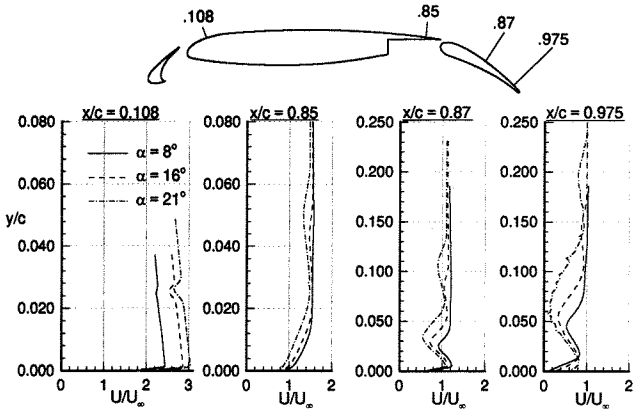

Figure 7: Main Element and Flap Velocity Profiles

In order to describe first-order effects of the spreading and merging wakes above the flap, a pseudo displacement thickness which includes wake deficits has been defined in terms of an integral of the difference between the measured profiles and corresponding inviscid profiles (based on the freestream stagnation pressure and the smoothed static-pressure distribution) and reference conditions evaluated at the centroid of the mass flux deficit. The variation of this displacement thickness with increasing angle of attack is illustrated in Figure 8 for five longitudinal stations on the flap (upper surface).

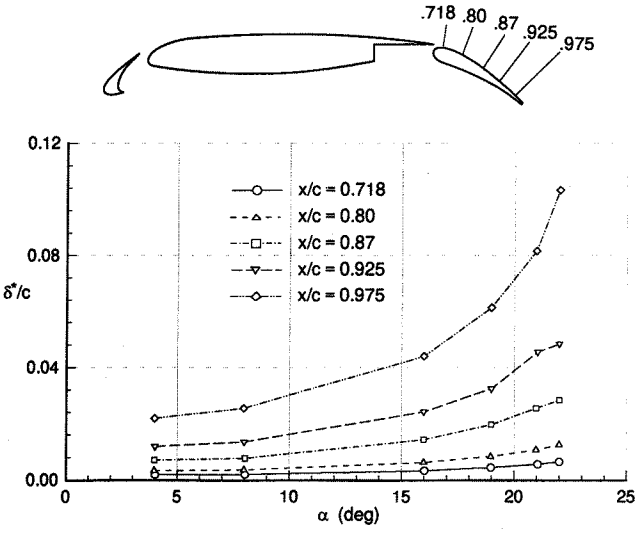

Figure 8: Displacement-Thickness Variation

Of most significance is the rapid increase in displacement thickness with increasing angle of attack at the aft-most survey station on the flap. It is surmised that this is the type of behavior leading up to the flap/main element unloading which is limiting maximum lift.

After this review of the experimental database for the baseline multielement high-lift airfoil geometry, it seems reasonable to conclude that the most important aerodynamic characteristics which must be accurately predicted for a variety of high lift geometries if a CFD design method is to be useful, and that can be addressed two-dimensionally initially, include the following:

- The flow breakdown on the flap and subsequent unloading of the aft portion of the main element caused by rapidly spreading and merging shear layers and wakes.
- Possible flow separation on the flap upper surface at approach conditions.
- Reynolds number effects.
- Compressibility effects on the slat.
- Boundary-layer transition characteristics including receptivity effects.

CFD METHOD(S)

Considering the complexity of the previously-delineated flow physics issues which must be properly addressed in order to provide an effective CFD method for the design of cost- and performance-effective 3-D high-lift systems, the selection of a Reynolds-averaged Navier-Stokes (RANS) method as the minimum acceptable fidelity level appears to be an unchallengeable choice[17]. A significant number of different RANS methods have been proposed and are being employed to analyze multielement high lift designs. Included amongst these are structured grid methods with varying grid strategies (i.e., overlapping, point mismatch, and point match), unstructured grid methods with different grid topologies, flow solvers employing either central-difference or upwind-differencing schemes, different turbulence models, different transition models, compressible and incompressible methods, etc. Although a compressible, structured-grid method employing multigrid, overlapping, solution-adaptive grids, an upwind differencing scheme, and a one-equation turbulence model, may be the current front-runner as the method of choice for practical and effective analysis and design of 3-D high-lift systems, the objectives of the 2-D assessment being addressed herein could be achieved using any one of the number of 2-D RANS methods currently in use. Rather than attempt to compare the results of numerous flow solvers here, a more detailed representative sample of some of the existing high-lift challenges are illustrated using one particular code, although most of the implications are common to most codes.

The compressible, unstructured-grid RANS code, NSU2D[18-21] was used for this study because it has proven to be quite efficient in terms of both user and computation time, and solutions appear to be in good agreement with various other codes. The version employed to generate the results presented in this paper allows for rapid generation of grids using an advancing layer/advancing front approach, incorporates an agglomeration multigrid method which does not require the user to generate grids for all levels of the multigrid sequence, and provides for node clustering including viscous clustering for both surface boundary layers and wakes. An illustration of a typical grid is provided in Figure 9. The spatial discretization scheme applies a finite-element formulation with central differencing of the convective terms. An explicit Runge-Kutta time stepping routine marches the solution to steady state, and closure of the RANS equations is accomplished using the Spalart-Allmaras one-equation turbulence model[22] for all the cases presented in this paper. Convergence is also accelerated by using residual smoothing and local time stepping.

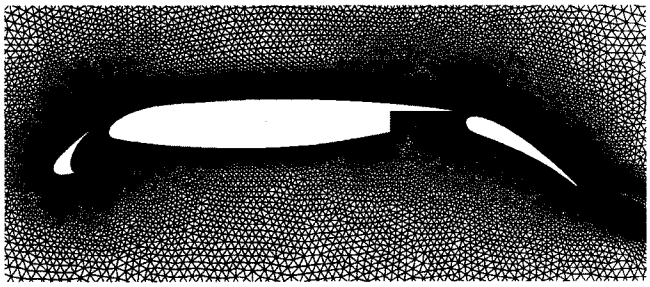

a) Three Element Airfoil

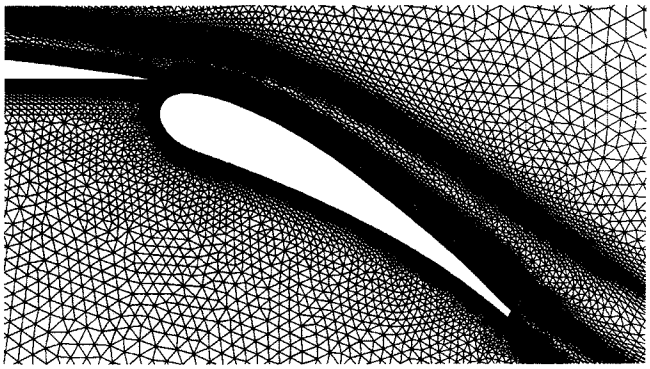

b) Flap Close-Up

Figure 9: Typical Multielement Airfoil Grid

Numerous grid studies with grids having up to 360,000 nodes have revealed that approximately 100,000 nodes, including sufficiently dense clustering of on- and off-body viscous regions, provide both low solution time and good accuracy. Coarser meshes tend to dissipate gradients excessively (often fortuitously bringing wake velocity deficit levels closer to experimental data), whereas higher density meshes and finer clustering in wake regions tend to exaggerate wake deficits. Typical setup and run times are currently "reasonable" with this code for use as a research tool. For a typical 100,000 node mesh (including 400 nodes on the main element, and 300 nodes on both the slat and flap), about 20 minutes on a workstation is needed to generate the grid, and solutions take about 45 minutes on a Cray C-90 (or about nine hours on a 100 MHz workstation). However, cases involving significant flow separation/reversal can require 2-3 times as many iterations to reach acceptable convergence levels.

Boundary-layer transition locations in NSU2D must currently be specified by the user. Laminar regions are modeled by turning off the source term in the turbulence model in the region between specified transition points (on the upper and lower surfaces of each element), so eddy viscosity is not generated there, but eddy viscosity from upstream turbulence is allowed to convect into the region. For the studies reported herein, transition locations have been specified to match the experimental indications of transition shown in Figure 5 for an almost identical geometry at the same conditions in the LTPT.

Another very important requirement for meaningful calibrations of CFD predictions with corresponding wind-tunnel test results is the modeling of the wind-tunnel walls (floor and ceiling in 2-D). For this study, a relatively simplified modeling is used. Parallel walls with inviscid boundary conditions model the floor and ceiling of the tunnel, and entrance and exit conditions are placed 20 chord lengths away from the model (as was done for the freestream outer boundary), to reduce the effects of these boundaries on the airfoil flow. No correction has yet been made for solid blockage.

CFD CALIBRATION - BASELINE GEOMETRY

A comparison of predicted component and total lift characteristics (both with and without the tunnel walls modeled) with the corresponding experimental results from two separate test entries in the LTPT is shown in Figure 10. Overall, the agreement is quite good, but there are some discrepancies. Considering the predictions with the wind-tunnel walls modeled, the following deviations are noted:

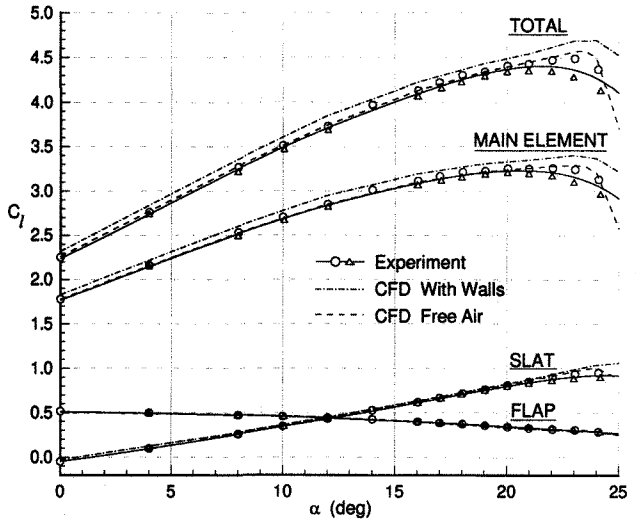

Figure 10: Comparison of Measured and Predicted Lift

- The predicted angle of attack for maximum lift is 2-3° higher than measured.
- The predicted maximum lift is about 5 percent higher than measured.
- The predicted lift level in the approach condition angle-of-attack range is slightly higher than the experimental indication.

It can be seen that the discrepancy between predicted and measured lift levels near maximum lift conditions is about equally split between the slat and main-element component contributions. However, the possibility that some significant portion of these deviations, as well as the differences at lower angles of attack, might well be a bias introduced in the pressure integrations by the use of relatively dense computational grids compared to the much coarser distribution of pressure orifices in the wind-tunnel model, will have to be considered. The overall surface "grid" density is different by a factor of nearly eight, and such a difference would likely introduce the greatest bias (toward higher computational lifts) in regions with relatively sharp (suction) pressure peaks, such as those which occur on the slat (and somewhat on the main element) at the higher angles of attack. However, any such biases do not explain the 2-3° difference in angle of attack for maximum lift.

Another characteristic worthy of note is the much more abrupt drop in lift beyond the maximum lift point predicted for the free-air case compared to the predictions with the wind-tunnel walls modeled. Although experimental results are not available that would allow us to validate the predicted trend at this time, this predicted trend bears further study.

Further insight into the underlying causes for the differences between the measured and predicted maximum lift levels and characteristics can be gained by examining the corresponding comparisons of the main element and flap normal-force distributions illustrated in Figures 11 and 12, respectively. Looking first at the predictions with wind-tunnel walls modeled, it can be seen that the predicted flow breakdown eventually experienced on the flap, although similar in character to that observed in the experiments, occurs at a higher angle of attack, and is perhaps a bit less severe judging from the reduced flattening of the upper-surface pressure distribution. The resultant unloading predicted for the aft portion of the main element is quite similar to that observed experimentally, other than it occurs at the higher angle of attack. Hence, it is concluded that the overall character of the eventual flow breakdown limiting maximum lift is adequately captured by the CFD prediction, but it occurs at a somewhat higher angle of attack.

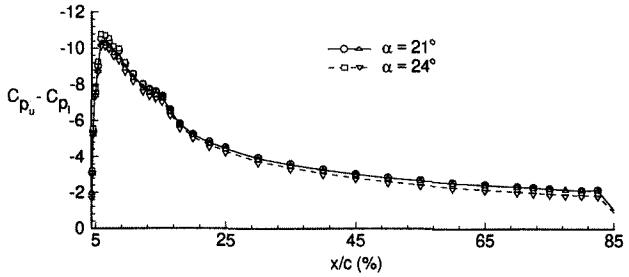

a) Experiment

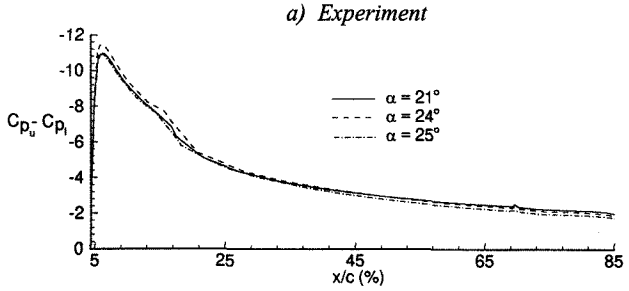

b) CFD With Walls Modeled

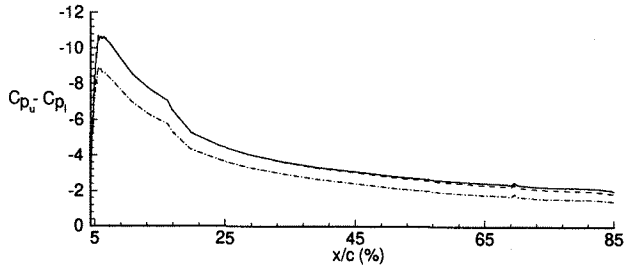

c) CFD Without Walls

Figure 11: Main Element Normal-Force Distributions

It is again worth noting the more exaggerated flow breakdown and resultant unloading predicted for the free-air case compared to the predictions with

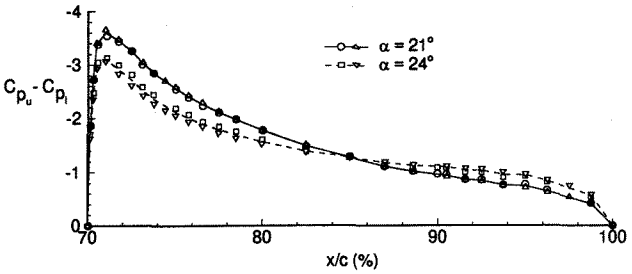

a) Experiment

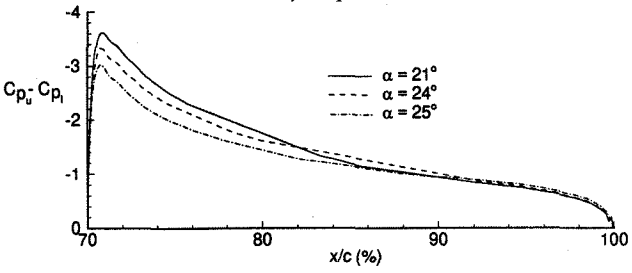

b) CFD With Walls Modeled

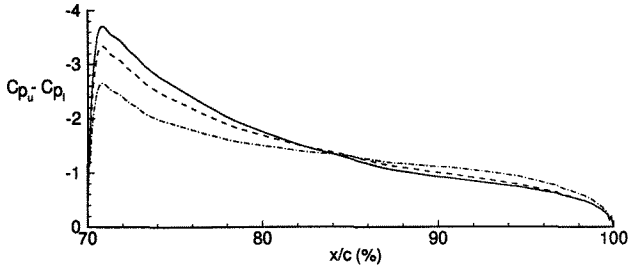

c) CFD Without Walls

Figure 12: Flap Normal-Force Distributions

tunnel walls modeled. A more severe breakdown (i.e., greater flattening of the pressure distribution) is predicted for the flap, and the resultant unloading predicted for the main element is significantly greater, and extends all the way to the leading edge of the main element.

Some of the more detailed diagnostic data available are examined next to see if explanations are forthcoming to explain the differences between CFD and experiment noted from the surface-pressure integrations and distributions. Comparisons of predicted and measured upper-surface skin-friction characteristics near the trailing edge of the main element, and at the two locations on the flap previously identified (in Figure 6), are presented in Figure 13. The following differences can be seen:

- Near the trailing edge of the main element, both sets of predictions overestimate the skin-friction-coefficient reductions with increasing angle of attack, thereby greatly exaggerating the potential for surface flow reversal at this location. It is interesting to note that the predictions with the tunnels walls modeled exhibited the greatest error.

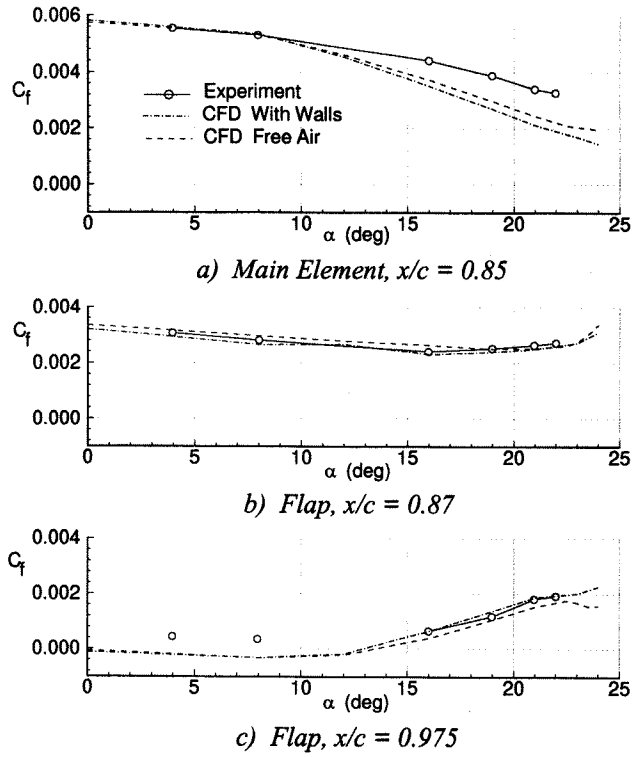

a) Main Element, x/c = 0.85

b) Flap, x/c = 0.87

c) Flap, x/c = 0.975

Figure 13: Comparison of Measured and Predicted Skin Friction Coefficients

- At the first station on the flap, both sets of predictions are in excellent agreement with the measured characteristics.
- At the station close to the flap trailing edge, both sets of predictions are also in excellent agreement with the experimental results at the higher angles of attack, with clearly no indication of surface flow reversal. However, at the lower (approach condition) angles of attack, both sets of predictions indicate some flow reversal, whereas the experimental measurements do not, albeit they reflected conditions quite close to separation.

Hence, there do not appear to be any insights gained from these data which would help explain the aforementioned deviations, especially at maximum lift conditions.

Turning next to the displacement-thickness indications which are derived from an integration of the boundary-layer and wake deficits, a comparison of these measured and predicted values at the same two flap stations is shown in Figure 14. It can be seen that both sets of predictions indicate higher values at maximum lift conditions than observed experimentally, and the predicted values with the tunnel walls modeled are in general greater than the free-air predictions. Both observations are somewhat contrary to expectations based on the

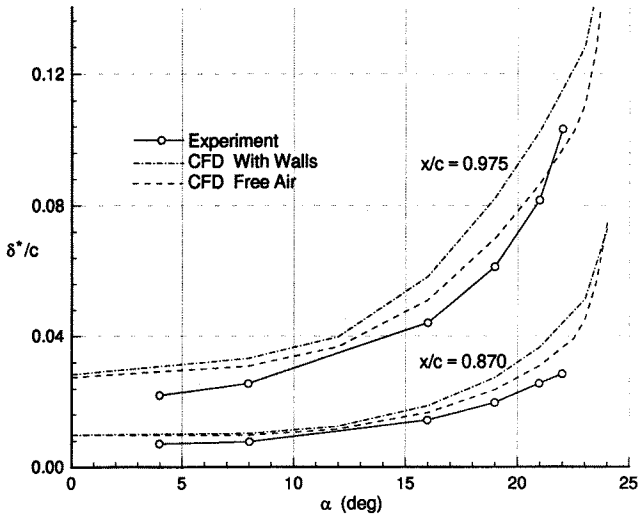

Figure 14: Comparison of Measured and Predicted Displacement Thickness

differences in lifting characteristics derived from the surface pressure data at maximum lift conditions, although the higher values at lower angles of attack seen in the predictions are consistent with the predicted flow reversal at the aft flap station.

Lastly, comparisons of the predicted and measured off-body velocity profiles at the same two flap stations have been examined. Relevant observations which can be derived from these comparisons, which are illustrated in Figures 15 and 16 for a range of angles of attack, are as follows:

- The magnitude of the predicted maximum velocity deficit is somewhat exaggerated more often than not for both the slat and main element wakes. This tendency is, in general, more pronounced when the wind tunnel walls are modeled.
- The predicted width (spreading) of these wakes is also somewhat exaggerated, with the discrepancy becoming significantly larger at higher angles of attack, especially at the aft flap station.
- At respective maximum lift conditions (higher angles of attack for the predictions), the predicted main element wake deficits are somewhat larger than the corresponding experimental definitions, but the predicted slat wake deficits are much greater than their experimental counterparts.

Consistent with the conclusions reached after examining the displacement-thickness differences, these data also appear to provide no additional insight into the mechanisms leading to the higher maximum-lift predictions. Hence, no insights are gained from examining any of the normal time-

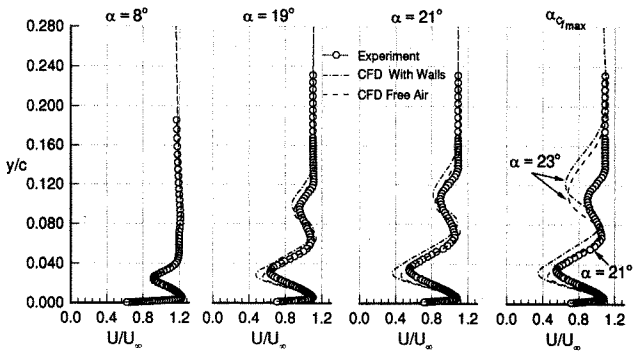

Figure 15: Comparison of Measured and Predicted Velocity Profiles at x/c = 0.87

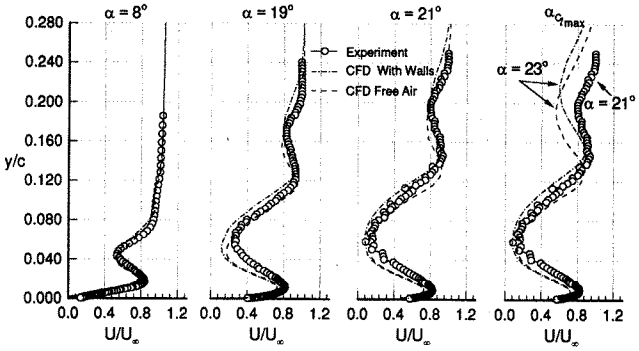

Figure 16: Comparison of Measured and Predicted Velocity Profiles at x/c = 0.975

averaged results that would help explain the observed differences between measured and predicted maximum lift characteristics. However, encountering discrepancies in the predicted wake characteristics does not come as a big surprise. Some very preliminary measurements of Reynolds stress components (u'v') have indicated much higher levels in the main element wake than present in the predictions with the existing one-equation turbulence model employed in this CFD calibration study. This is an area that is now being investigated further.

CFD CALIBRATION - GEOMETRY CHANGES

Accuracy in predicting absolute aerodynamic characteristics is clearly very important, but perhaps even more important is the reliable prediction of the incremental aerodynamic changes due to configuration changes. Determination of these sensitivities is a major portion of the subsonic transport design and development process for high-lift systems, whether it be for component rigging studies or overall configuration optimization. Therefore, if aerodynamic design cycle times are to be reduced substantially as desired, then CFD methods must be developed to the point where they can quickly provide reliable predictions of the various sensitivities required. Such reliable CFD methods can also provide much more insight into the complex flow physics governing 3-D high-lift system performance than can ever be provided experimentally, and hence should prove to be invaluable in providing the guidance needed to develop high-lift system designs which are more optimum, considering cost, performance, complexity, and many other factors.

In order to assess the current status/reliability of state-of-the-art 2-D CFD methods for predicting such sensitivities, two representative configuration changes have been selected for analysis and subsequent comparison with a relatively large corresponding experimental database. One of these is a relatively simple flap rigging change where the flap-to-spoiler gap is opened up somewhat in an attempt to reduce the merging between the main element wake and the flap boundary layer, with the intention of improving the maximum lift capability. In this case, the flap gap/overhang rigging is changed from the baseline (1.27%c/0.25%c) to 1.50%c/0.25%c. The second configuration change involves increasing the flap deflection from the baseline value of 30° (with the 1.27%c/0.25%c rigging) to 35°, with flap rigging of 0.95%c/0%c. This configuration change would be a normal part of a typical optimization process examining maximum lift capability as well as lift and drag at approach conditions, as a minimum.

Comparison of the CFD predicted and the measured incremental lift characteristics for the flap rigging change are shown in Figure 17. Both the total lift change as well as the flap contribution are

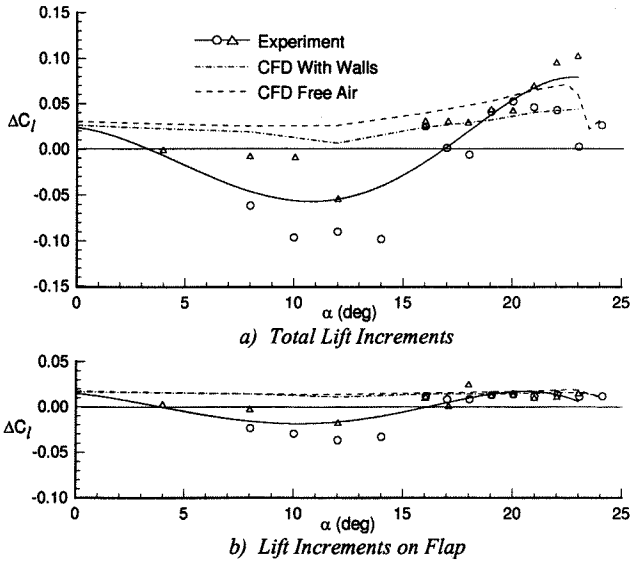

Figure 17: Comparison of Measured and Predicted Lift Increments for Increased Flap Gap

illustrated. Experimental values are shown from two separate test entries. Important observations and conclusions which can be drawn from this comparison include:

- The CFD predictions largely duplicate the experimentally observed increase in lift at the higher angles of attack around maximum lift conditions.
- The CFD predictions do not capture the lift loss observed experimentally at the lower, approach-condition angles of attack which is caused by flow separation on the flap with this larger gap, which, in turn, unloads the main element.

Corresponding CFD-predicted and measured skin-friction characteristics on the main element and flap are displayed in Figure 18. It is important to note

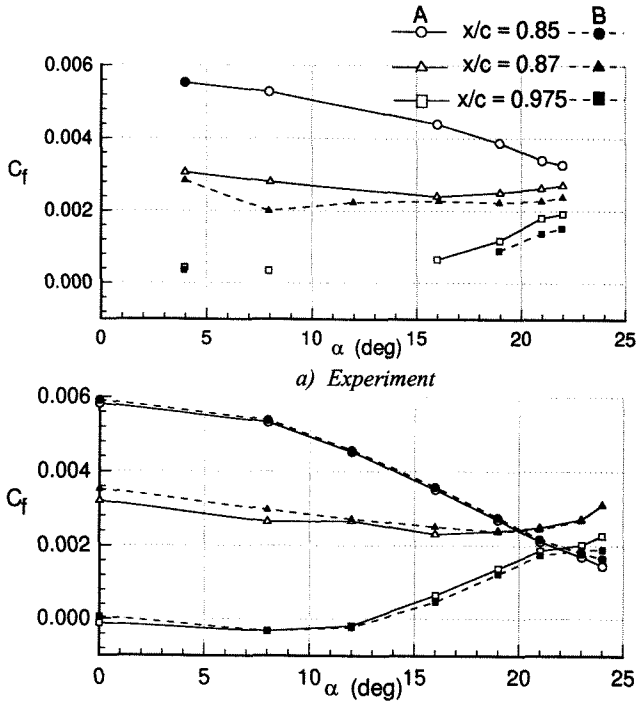

a) Experiment

b) CFD With Walls Modeled

Figure 18: Effect of Increased Flap Gap on Skin Friction Characteristics

that the absence of experimental results at the aft station on the flap at 8°, 12° and 16° angle of attack is an indication that flow reversal was encountered at these conditions, but the data obtained with the flat-tube pitot probe at these conditions does not permit any assessment of the magnitude of the surface flow reversal. By comparing the experimental and CFD-predicted trends (with the tunnel walls modeled), it can be seen that the CFD method is not duplicating the experimentally-observed flow deterioration on the flap surface produced by increasing the flap gap (i.e., B vs. A).

An examination of the measured and predicted off-body flow field changes produced by this flap rigging change produces some curious results. Measured and CFD-predicted displacement thicknesses for both the baseline and re-rigged flap geometries are illustrated in Figure 19 for the standard two stations on the flap, and corresponding

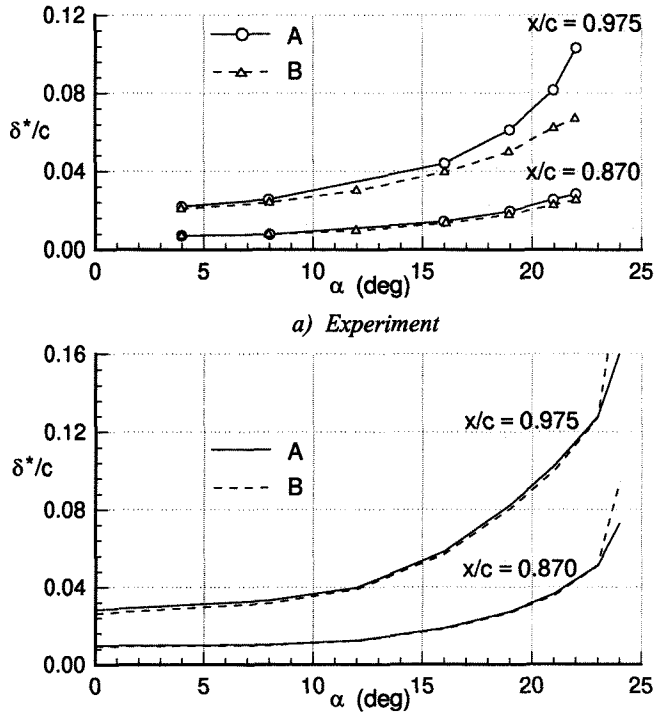

a) Experiment

b) CFD With Walls Modeled

Figure 19: Effect of Increased Flap Gap on Displacement Thickness Characteristics

measured and predicted velocity profiles for both configurations are presented in Figure 20 for the aft station on the flap. From the experimental results, it can be seen that increasing the flap gap did produce the desired reduction in displacement thickness at the higher angles of attack approaching maximum lift conditions. And, it can be seen that the main element wake is significantly smaller at maximum lift conditions. Qualitatively, these trends would help explain the observed maximum lift increase. On the other hand, the corresponding CFD predictions (shown with wall effects modeled, although free-air trends are the same) do not suggest the reduction in main element wake size and ensuing reduction in displacement thickness at maximum lift conditions. Yet, the CFD-predicted improvement in maximum lift is the same as that measured. These results tend to produce suspicions that the agreement for maximum lift improvement could well be fortuitous. This possibility will have to be explored.

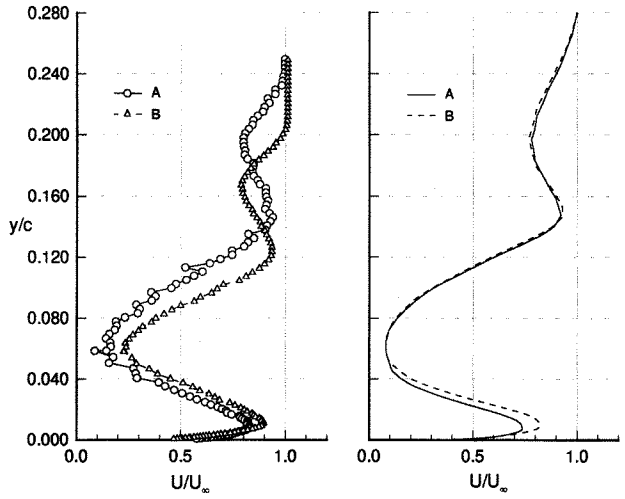

a) Experiment *b) CFD With Walls Modeled*

Figure 20: Effect of Increased Flap Gap on Velocity Profiles at x/c = 0.975, α = 21°

Turning next to the test case where the flap deflection is increased, comparisons of the CFD-predicted and experimentally-measured incremental lift changes for this geometry modification are shown in Figure 21. Again, two sets of experimental data from different test entries are available. For this

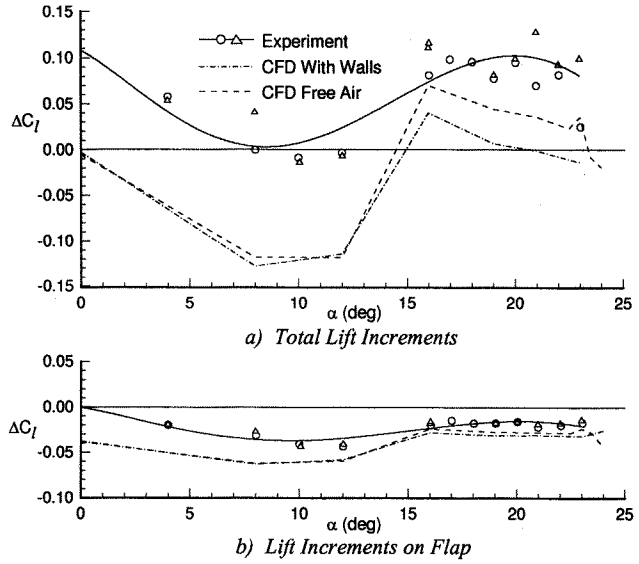

a) Total Lift Increments

b) Lift Increments on Flap

Figure 21: Comparison of Measured and Predicted Lift Increments for Increased Flap Deflection

case, it can be seen that the CFD predictions (especially with the tunnel walls modeled) completely miss the experimentally observed improvement at maximum lift conditions, and also indicate a significant loss in lift at approach conditions not observed in the experiments. The only positive statement that can be made about the predictions is that the trend between approach and maximum-lift incremental changes is captured, but that is obviously not enough.

The measured and CFD-predicted skin-friction characteristics for these two configurations are presented in Figure 22. In this case, contrary to the results seen for the flap rigging change, CFD predictions significantly exaggerate the flow deterioration on the flap surface produced by the increased flap deflection (i.e., C vs. A), particularly at the first station on the flap.

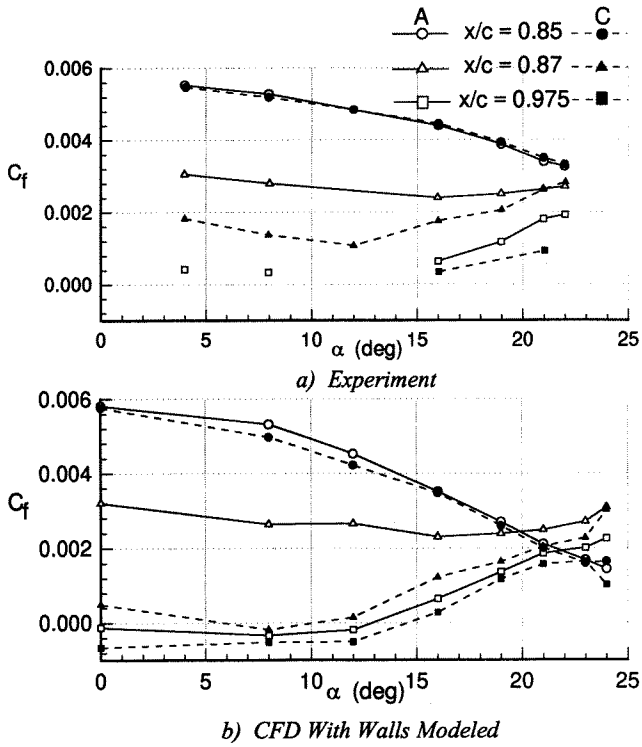

a) Experiment

b) CFD With Walls Modeled

Figure 22: Effect of Increased Flap Deflection on Skin Friction Characteristics

An examination of the measured and predicted off-body flowfield changes produced by this increase in flap deflection also presents some interesting results. In comparing the measured and predicted displacement thickness characteristics shown in Figure 23 for both configurations at the two standard stations on the flap, it can be seen that, in this case, the CFD predictions exaggerate the growth caused by the increased deflection. This is somewhat contrary to the significant underprediction of the growth for the flap rigging change. Consistent with the displacement thickness results, it can be seen in Figure 24 that the CFD predictions clearly exaggerate the growth of the main element wake at maximum lift conditions with increasing flap deflection.

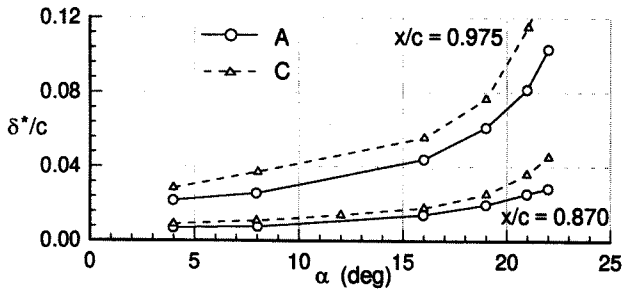

a) Experiment

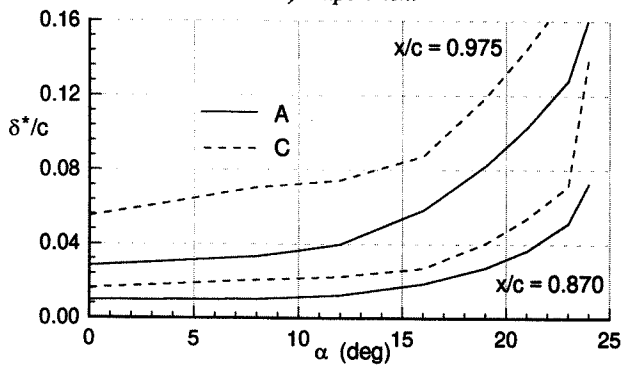

b) CFD With Walls Modeled

Figure 23: Effect of Increased Flap Deflection on Displacement Thickness Characteristics

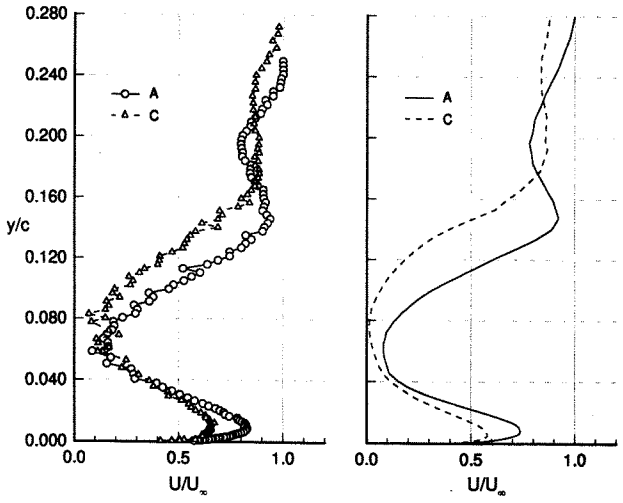

a) Experiment *b) CFD With Walls Modeled*

Figure 24: Effect of Increased Flap Deflection on Velocity Profiles at x/c = 0.975, α = 21°

CONCLUSIONS

A major effort is now being focused on the development of effective CFD capabilities for analyzing complex 3-D high-lift systems including engine installation effects in order to permit a large reduction in the aerodynamic design cycle time required, and to make it possible to define more cost- and performance-effective concepts. A few key enabling technologies have been selected for significant focused effort. One of these is the development of turbulence models appropriate to represent the very complex flow physics involved. To assess the current status of state-of-the-art CFD methods to adequately represent some of these complex flow situations, results from a comprehensive 2-D experimental program investigating multielement high-lift airfoil characteristics, including extensive diagnostic measurements, and corresponding CFD (RANS) calibration studies have been reviewed. Conclusions derived from this assessment are as follows:

1. Experimental results clearly illustrate that the characteristics of merging and spreading shear layers and wakes above the flap control the level of maximum lift achievable, and configuration changes which either increase or diminish this spreading and merging produce relatable performance changes.
2. RANS CFD predictions obtained with a state-of-the-art one-equation turbulence model closely approximate the overall flow mechanism limiting maximum lift, but do not adequately capture changes due to configuration modifications which influence these merging and spreading shear layers and wakes.
3. Experimental results illustrate that flow separation on the flap upper surface at approach conditions is often a limiting factor in establishing appropriate flap riggings, but the RANS CFD predictions of this flow phenomenon are not at all reliable.

It is therefore concluded that significant additional attention must be placed on improving the reliability of RANS methods for predicting these flow characteristics at 2-D conditions before it would be warranted to attempt a full 3-D version. 2-D experimental and analytical studies to guide the development of more appropriate turbulence models are clearly warranted.

REFERENCES

1. Rubbert, P.E., "CFD and the Changing World of Airplane Design," ICAS-94-0.2, Sept. 1994.
2. Lynch, F.T. and Intemann, G.A., "The Modern Role of CFD in Addressing Airframe/Engine Integration Issues for Subsonic Transports," ICAS-94-6.4.3, Sept. 1994.
3. Valarezo, W.O., Dominik, C.J., McGhee, R.J., Goodman, W.L., and Paschal, K.B., "Multielement Airfoil Optimization for Maximum Lift at High

Reynolds Numbers," AIAA Paper 91-3332, Sept. 1991.

4. Lynch, F.T., "Experimental Necessities for Subsonic Transport Configuration Development," AIAA Paper 92-058, Jan. 1992.
5. Valarezo, W.O., Dominik, C.J., McGhee, R.J., and Goodman, W.L., "High Reynolds Number Configuration Development of a High-Lift Airfoil," AGARD CP-515, Paper No. 10, 71st AGARD FDP Symposium on High-Lift System Aerodynamics, Banff, Alberta, Oct. 1992.
6. Valarezo, W.O., "High Lift Testing at High Reynolds Numbers," AIAA Paper 92-3986, July 1992.
7. Valarezo, W.O., "Topics in High-Lift Aerodynamics," AIAA Paper 93-3136, July 1993.
8. Chin, V.D., Peters, D.W., Spaid, F.W., and McGhee, R.J., "Flowfield Measurements About a Multi-Element Airfoil at High Reynolds Numbers," AIAA Paper 93-3137, July 1993.
9. Nakayama, A., Stack, J.P., Lin, J.C., and Valarezo, W.O., "Surface Hot-Film Technique for Measurements of Transition, Separation, and Reattachment Points," AIAA Paper 93-2918, July 1993.
10. Lynch, F.T., Crites, R.C., and Spaid, F.W., "The Crucial Role of Wall Interference, Support Interference, and Flow Field Measurements in the Development of Advanced Aircraft Configurations," AGARD-CP-535, Paper No. 1, Oct. 1993.
11. Lynch, F.T., "Subsonic Transport High-Lift Technology — Review of Experimental Studies," AIAA Overview of High Lift Aerodynamics, June 1995.
12. Spaid, F.W., and Lynch, F.T., "High Reynolds Number, Multi-Element Airfoil Flowfield Measurements," AIAA Paper 96-0682, Jan. 1996.
13. McGhee, R.J., Beasley, W.D., and Foster, J.M., "Recent Modifications and Calibration of the Langley Low-Turbulence Pressure Tunnel," NASA TP2328, 1984.
14. Paschal, K., Goodman, W., McGhee, R., Walker, B. and Wilcox, P.A., "Evaluation of Tunnel Sidewall Boundary-Layer-Control Systems for High-Lift Airfoil Testing," AIAA Paper 91-3243, Sept. 1991.
15. Klausmeyer, S.M., and Lin, J.C., "An Experimental Investigation of Skin Friction on a Multi-Element Airfoil," AIAA Paper 94-1870, June 1994.
16. Clauser, F.H., "Turbulent Boundary Layers in Adverse Pressure Gradients," J. Aero. Sci., Vol. 21, Feb. 1954, pp. 91-108.
17. Ying, S.X., "High Lift: Challenges and Directions for CFD," Proceedings AIAA/NPU AFM Conference, June 1996.
18. Mavriplis, D.J., Jameson, A., and Martinelli L., "Multigrid Solution of the Navier-Stokes Equations on Triangular Meshes," AIAA Paper 89-0120, Jan. 1989.
19. Mavriplis, D.J., "Turbulent Flow Calculations Using Unstructured and Adaptive Meshes," International Journal for Numerical Methods in Fluids, Vol. 13, 1991, pp. 1131-1152.
20. Mavriplis, D.J., and Venkatakrishnan, V., "A 3-D Agglomeration Multigrid Solver for the Reynolds - Averaged Navier-Stokes Equations on Unstructured Meshes," AIAA Paper 95-0345, Jan. 1995.
21. Valarezo, W.O., and Mavriplis, D.J., "Navier-Stokes Applications to High-Lift Airfoil Analysis," AIAA Paper 93-3534, Aug. 1993.
22. Spalart P.R., and Allmaras, S.R., "A One-Equation Turbulence Model for Aerodynamic Flows," AIAA Paper 92-0439, Jan. 1992.